Probing High Momentum Protons and Neutrons in Asymmetric Nuclei

The CLAS Collaboration

The atomic nucleus is one of the densest and most complex quantum-mechanical systems in nature. Nuclei account for nearly all the mass of the visible universe. The properties of individual protons and neutrons (nucleons) in nuclei can be studied by scattering a high-energy particle from the nucleus and detecting this particle after it scatters, often also detecting an additional knocked-out proton. Analysis of electron and proton scattering experiments suggests that part of the nucleons in nuclei form close-proximity neutron-proton (np) pairs [1-12]. Nucleons in these pairs have high-momentum, greater than the nuclear Fermi momentum (k_F). We measured protons and, for the first time, neutrons knocked out of medium to heavy nuclei by high-energy electrons. Here we show that the fraction of high-momentum protons increases dramatically with the neutron excess, while the fraction of high-momentum neutrons decreases slightly. This effect is surprising, since in the classical nuclear shell model protons and neutrons obey Fermi statistics, have little correlation, and mostly fill independent energy shells. These high-momentum nucleons in asymmetric nuclei are important to understand nuclear parton distribution functions (the EMC Effect) [1, 13-14]. They are also relevant for interpretation of neutrino oscillation measurements [15] and understanding of neutron rich systems such as neutron stars [4, 16].

Since the 1950s, the independent particle shell model has been an indispensable guide for understanding nuclei [17]. In this model, nucleons move independently in well-defined quantum orbits (shells) with low momentum ($k < k_F$), similarly to electrons in atoms. The potential in which the nucleons move is the average nuclear field created by their strong mutual interactions. While successful in making many important predictions, this textbook picture of the nucleus is quite incomplete: electron scattering experiments in nuclei ranging from lithium to lead measured only about 60%–70% of the expected number of protons in each shell [18]. Newer shell-model type calculations include the effects of long range correlations, increasing this to about 80% [19].

Modern superconducting accelerators, with high-energy, high-intensity, and high-duty-factor, allow experiments that use scattering reactions to resolve the structure and dynamics of individual nucleons and nucleon pairs in nuclei. The measurement's resolving power is determined by its momentum transfer and its interpretation relies on the theoretical modeling of the interaction that should account for all possible mechanisms that lead to the same measured final state. The high-momentum transfer measurements reported here are discussed in terms of interaction with single nucleons, which is the simplest reaction picture that is consistent with the measured observables [1-4] and various ab-initio calculations [20].

Analyzed within this picture, electron scattering experiments suggest that about 20% of the nucleons in nuclei have momentum greater than the nuclear Fermi momentum, k_F [1-4, 10-12]. These nucleons are absent in the one-body shell model description of the data and are coupled into short-lived correlated nucleon-pairs with large relative momentum ($k_{relative} > k_F \approx 250$ MeV/c) and small center-of-mass (CM) momentum ($k_{CM} < k_F$), referred to as short-range correlated (SRC) pairs [1-4].

The dominant force between the nucleons in the SRC pairs is tensor in nature [1-2]. This pair-wise interaction acts predominantly on spin-1 np-SRC pairs, leading to a predominance of np-SRC pairs over proton-proton (pp) and neutron-neutron (nn) SRC pairs by a factor of about 20. This phenomenon is referred to as "np-dominance" [1-9].

Almost all high-momentum nucleons in nuclei belong to an SRC pair. As the short-distance interaction between nucleons in SRC pairs is very strong, the characteristics of the resulting pairs are largely independent of the rest of the nucleus. Thus, the distribution of high-momentum nucleons (the "high-momentum tail") has a universal shape for all nuclei [1-4, 10-12, 21].

SRC pairs significantly complicate the nuclear ground state and nuclear structure calculations. From a theoretical point of view, one can use a unitary transform to shift this complexity from the ground state to many-body interaction operators that describe the same measured final state [22, 23], shifting the physics from high-momentum correlations to short-distance operators. The physical pictures of high-momentum nucleons / short-distance operators share the use of scale separation of these effects from the shell-model scales. The new results reported here constrain the short-distance phenomena, as described in either framework.

The analysis reported here was motivated by the quest to study the short-distance dynamics of protons and neutrons in neutron-rich nuclei. For the first time, we simultaneously measured electron-induced quasi-elastic (QE) knockout of protons and neutrons from medium and heavy nuclei, using the A(e,e'p) and A(e,e'n) reactions, respectively. The simultaneous measurement of both proton and neutron knockout is the unique feature of this work that allows us to directly compare their properties using minimal assumptions. Analyzed within the one-body reaction picture, the data from these measurements perform four functions: (1) quantifying the relative fractions of high-momentum ($k > k_F$) protons and neutrons, (2) showing that adding *neutrons* to the nucleus
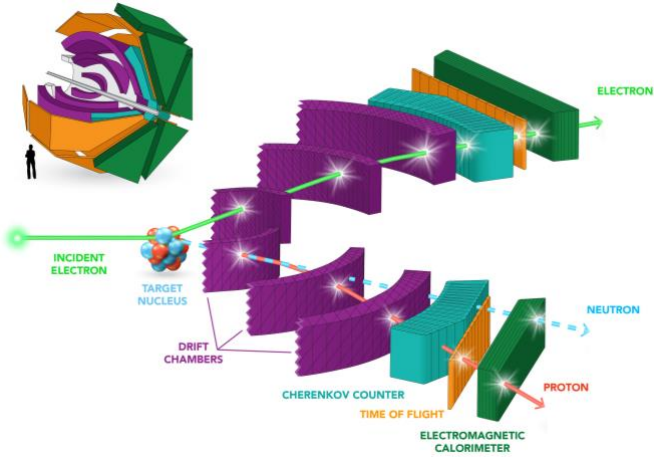
Fig 1 | The CLAS Spectrometer. Main image: Two segments of CLAS. Electrons traveling with energies up to 6 billion electron volts hit nuclei, knocking out individual protons and neutrons. The momenta of the scattered electrons and knocked-out protons are reconstructed by analyzing their trajectories as they bend in a toroidal magnetic field. The neutron momenta are deduced from their time of flight until they interact with the electromagnetic calorimeter. Inset: the almost spherical CLAS. The electron beam travels along the gray pipe, hitting a target near the center of the spectrometer.

increases the fraction of high-momentum *protons*, (3) helping confirm the np-SRC dominance of the high-momentum tail in medium and heavy nuclei, and (4) supporting momentum-sharing inversion in heavy nuclei. In a more general framework, the data show that short-distance dynamics is similar in all nuclei, supporting a scale separation of short-distance physics from the nuclear shell model.

The data presented here were collected in 2004 in Hall-B of the Thomas Jefferson National Accelerator Facility (Jefferson Lab) in Virginia, USA, and are reanalyzed here as part of the Jefferson Lab data-mining initiative. The experiment used a 5.014 GeV electron beam incident on deuterium, carbon, aluminum, iron, and lead targets, and the CEBAF Large Acceptance Spectrometer (CLAS) [24] to detect the scattered electron and any associated hadrons knocked out during the interaction (see Fig. 1). CLAS used a toroidal magnetic field and six independent sets of drift chambers, time-of-flight scintillation counters, Cherenkov counters, and electromagnetic calorimeters, covering scattering angles from about 8° to 140° for charged-particle identification and trajectory reconstruction. The neutrons were identified by observing interactions in the forward electromagnetic calorimeters (covering about 8° to 45°) with no associated charged-particle tracks in the drift chambers. The angle- and momentum-dependent neutron detection efficiency and momentum reconstruction resolution were measured simultaneously using the $d(e,e'p\pi^+\pi^-n)$ reaction [25]. The experiment recorded all events with a scattered electron detected in both the electromagnetic calorimeter and the Cherenkov counter, along with any other particles.

High-energy electrons scatter from the nucleus by transferring a single virtual photon, carrying momentum $\vec{q}$ and energy ω. In QE scattering, this momentum transfer is absorbed by a nucleon with initial momentum $\vec{p}_i$. If the nucleon does not rescatter as it leaves the nucleus, then it will emerge with momentum $\vec{p}_N = \vec{p}_i + \vec{q}$. Thus, we can reconstruct the approximate initial momentum of the nucleon from the missing momentum, the difference between the detected nucleon momentum and the transferred momentum: $\vec{p}_{miss} = \vec{p}_N - \vec{q}$. Similarly, the excitation energy of the residual (A-1) nucleus is related to the missing energy, $E_{miss} = \omega - T_N$, where T_N is the nucleon's kinetic energy.

While this QE picture of the scattering reaction is highly intuitive, and consistent with the measured observables, other reaction mechanisms using two-body currents, that result in the same measured final state, add coherently and cannot be distinguished. Contribution from non-QE reaction mechanisms are minimized by the use of large momentum transfer and the specific reaction kinematics used in the measurement (see Methods). In addition, these effects are further diminished by forming ratios of cross sections.

In this analysis, we studied (e,e'p) and (e,e'n) QE knockout event samples measured in two kinematical regions, corresponding to electron scattering off high-initial-momentum ($p_i > k_F$) nucleons, presumably from an SRC pair, or from low-initial-momentum ($p_i < k_F$) nucleons, presumably from shell model states.

Using these event samples, we derived both the ratio of A(e,e'n)/A(e,e'p) events for each region and the double ratio of high-momentum (SRC) to low-momentum (shell-model) nucleons in nuclei relative to carbon, [A(e,e'N)$_{High}$ / A(e,e'N)$_{Low}$] / [^{12}C(e,e'N)$_{High}$ / ^{12}C(e,e'N)$_{Low}$]. Here N refers to either protons or neutrons, and A stands for either aluminum, iron, or lead. The double-ratio is simply an estimator for the increased fraction of SRC nucleons in an asymmetric nucleus compared to carbon. We use carbon as a reference since it is a well-studied, medium-mass, symmetric nucleus and has similar average density to the other measured nuclei. In addition, forming cross-section ratios relative to carbon significantly reduces the effects of detector acceptance and efficiency corrections [25].

For each kinematical setting, we used the same selection criteria on the detected scattered electron and associated knocked-out nucleon (proton or neutron) to select QE A(e,e'p) and A(e,e'n) events.

Low-initial-momentum events are characterized by low missing energy and low missing momentum ($E_{miss} <$ 80-90 MeV; and $p_{miss} = |\vec{p}_{miss}| < 250$ MeV/c) [25]. Because the neutron resolution was not good enough to select these events directly, we developed a set of alternative constraints to select the same events by using the detected electron momentum and the knocked-out nucleon angle, which were unaffected by the neutron momentum resolution (see Methods).

Similarly, we selected the high-initial-momentum events in two steps. We first selected QE events with a leading

nucleon by cutting on the energy and momentum transfer and requiring that the outgoing nucleon be emitted with most of the transferred momentum in the general direction of the momentum transfer. We then selected high-initial-momentum events by requiring large missing momentum ($p_{miss} > 300$ MeV/c). These selection criteria ensured that the electron interacted with a single high-initial-momentum proton or neutron in the nucleus [2-4]. Last, we optimized the nucleon-momentum dependent cuts to account for the neutron momentum reconstruction resolution and corrected for any remaining bin migration effects (see Methods).

To verify the neutron detection efficiency, detector acceptance corrections, and event selection method, we extracted the carbon neutron-to-proton reduced cross-section ratio for both high and low initial nucleon momenta: $[^{12}C(e,e'n)/\sigma_n] / [^{12}C(e,e'p)/\sigma_p]$ (i.e., measured cross-sections scaled by the known elastic electron-proton σ_p and electron-neutron σ_n cross-sections). Figure 2 shows these two measured cross-section ratios are consistent with unity, as expected for a symmetric nucleus. This shows that in both high- and low-initial-momentum kinematics we have restricted the reaction mechanisms to primarily QE scattering and have correctly accounted for the various detector-related effects.

For the other measured nuclei, the (e,e'n)/(e,e'p) low-momentum reduced cross-section ratios grow approximately as N/Z, as expected from simple nucleon counting. However, the (e,e'n)/(e,e'p) high-momentum ratios are consistent with unity for all measured nuclei, see Fig. 2.

The struck nucleons could reinteract as they emerged from the nucleus; we refer to that as Final State Interaction (FSI). Such an effect would cause the number of detected outgoing nucleons to decrease and also modify the angles and momenta of the knocked-out nucleons. These effects were estimated for symmetric and asymmetric nuclei using a relativistic Glauber framework which showed that the decrease in the measured cross section is similar for protons and neutrons and thus has a minor impact on cross-section ratios (see Methods).

Since rescattering changes the event kinematics, some of the events with high measured p_{miss} could have originated from electron scattering from a low-initial-momentum nucleon, which then rescattered, increasing p_{miss}. If the high-initial-momentum (high-p_{miss}) nucleons were caused by electron scattering from the more-numerous low-initial-momentum nucleons followed by nucleon rescattering, then the high-momentum (e,e'n)/(e,e'p) ratio would show the same N/Z dependence as the low-momentum ratio. As the high-momentum (e,e'n)/(e,e'p) ratio is independent of A, these nucleon-rescattering effects must be small in this measurement.

Thus, the constant (e,e'n)/(e,e'p) high-momentum ratios indicate that there are equal numbers of high-initial-momentum protons and neutrons in asymmetric nuclei, even though these nuclei contain up to 50% more
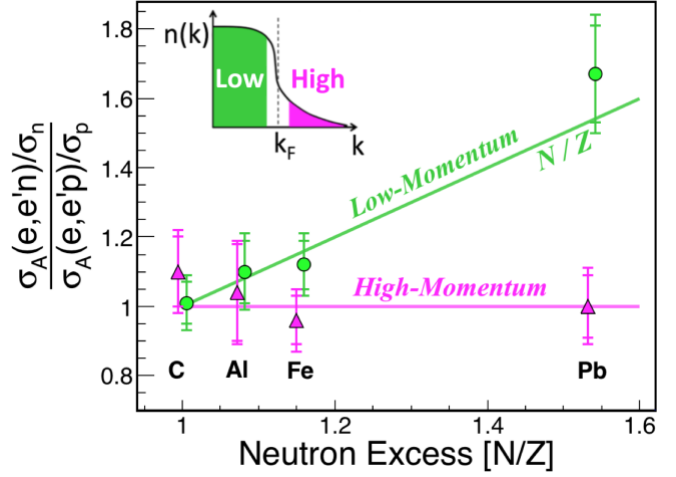

Fig 2 | The relative abundances of high- and low-initial-momentum neutrons and protons. $[A(e,e'n)/\sigma_n] / [A(e,e'p)/\sigma_p]$ reduced cross-section ratio for low-momentum (green circles) and high-momentum (purple triangles) events. The initial nucleon momenta corresponding to each type of event are illustrated in the inset. The lines show the simple N/Z expectation for low-momentum nucleons and the np-dominance expectation (i.e., ratio = 1) for high-momentum nucleons. The inner error bars are statistical while the outer ones include both statistical and systematic uncertainties [25].

neutrons than protons. This observation is consistent with high-initial-momentum nucleons belonging primarily to np-SRC pairs, even in neutron rich nuclei [27]. This number equality implies a greater fraction of high-initial-momentum protons. For example, if 20% of the 208 nucleons in lead-208 are at high-initial-momentum, then these consist of 21 protons and 21 neutrons. This corresponds to a high-momentum proton fraction of 21/82 ~ 25% and a corresponding neutron fraction of only 21/126 ~ 17%.

In order to quantify the relative fraction of high-momentum protons and neutrons in the different nuclei with minimal experimental and theoretical uncertainties, we extracted the double ratio of (e,e'N) high-initial-momentum to low-initial-momentum events for nucleus A relative to carbon for both protons and neutrons. We find that the fraction of high-initial-momentum protons *increases* by about 50% from carbon to lead (see Fig. 3).

Moreover, the corresponding fraction of high-initial-momentum neutrons seems to *decrease* by about $10 \pm 5\%$. Nucleon-rescattering, if significant, should increase in larger nuclei and should affect protons and neutrons equally (see Methods). Since, unlike the protons, the neutron ratio decreases slightly with A, this also rules out significant nucleon rescattering effects.

Fig. 3 also shows the results of a simple phenomenological (i.e., experiment-based) np-dominance model [6, 26] which uses a mean-field momentum distribution at low momentum ($k < k_F$) and a scaled deuteron-like high-momentum tail. This model agrees with our data and also predicts momentum-sharing
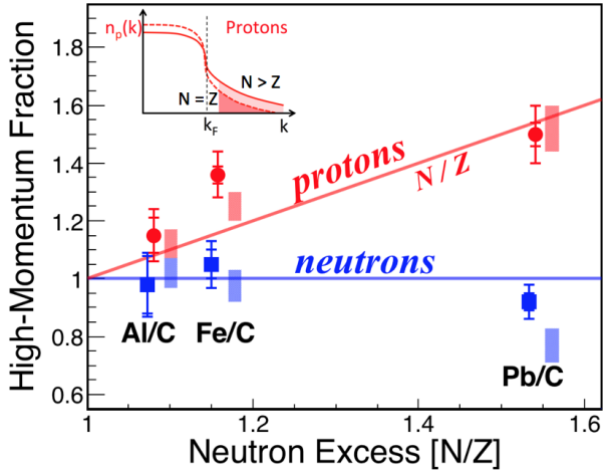
Fig 3 | Relative high-momentum fractions for neutrons and protons. Red circles: The double-ratio of the number of (e,e'p) high-momentum proton events to low-momentum proton events for nucleus A relative to carbon. The inner error bars are statistical while the outer ones include both statistical and systematic uncertainties. Red bands: the prediction of the phenomenological np-dominance model [25]. Blue squares and bands: the same for neutron events. The inset demonstrates how adding neutrons increases the fraction of protons in the high momentum tail. The red line at *N/Z* and the blue line at 1 are drawn to guide the eye.

inversion, i.e. on average, protons move faster than neutrons in neutron-rich nuclei.

These results indicate that high-momentum nucleons / short-range two-body currents are universal and independent of the shell-model. This conclusion holds for both the QE and unitary transformed pictures of the interaction and indicate that nuclei must be viewed in a scale-dependent way: nuclear structure at higher momentum scales / shorter distances must be described using universal two-body physics that is absent in an independent particle shell model picture using one-body operators.

The surprising fact that increasing the number of *neutrons* in a nucleus increases the fraction of high-initial-momentum *protons*, proposed by [26] and bolstered by exact calculations of light nuclei [27] and calculations of heavier nuclei [28] and asymmetric nuclear matter [29], has several broad implications. Neutron stars contain about 5 to 10% protons and electrons in their central layers. Our work implies that the extreme neutron excess in a neutron star could dramatically increase the effects of short-distance currents on the protons. This effect could impact the cooling rate and equation of state of neutron stars [4, 16].

There is evidence that the high-momentum nucleons associated with SRC pairs are responsible for the EMC effect, the change in the quark distribution of nucleons bound in nuclei [1, 13]. The EMC effect may result from two-body short-distance currents that can be viewed as temporary high-density fluctuations in the nucleus, in which the internal structure of the affected nucleons is briefly modified [1]. If this mechanism indeed occurs,

then the average proton in neutron-rich nuclei (the minority species) is more correlated and should therefore be more modified than the average neutron (the majority). Observing such increased modification of the proton structure in neutron rich nuclei could shed new light on the currently unknown origin of these modifications.

Furthermore, the np-dominance of short range correlated pairs and two-body short distance currents in heavy nuclei has significant implications in many areas of nuclear and particle physics, including nuclear correlation functions and the double beta decay rate of nuclei [30], the nature of the repulsive core of the nucleon-nucleon interaction [2, 7], and our understanding of neutrino-nucleus interactions, where future high precision extraction of oscillation parameters and searches for new physics beyond the standard model require detailed understanding of the nuclear ground state and the neutrino interaction operators [15].

1. O. Hen et al., Rev. Mod. Phys. **89**, 045002 (2017).
2. C.C. degli Atti, Phys. Rep. **590**, 1 (2015)
3. J. Arrington et al., Prog. Part. Nucl. Phys. **67**, 898 (2012).
4. L. Frankfurt, M. Sargsian, and M. Strikman, Int. J. Mod. Phys. A **23**, 2991 (2008).
5. R. Subedi et al., Science **320**, 1476 (2008).
6. O. Hen et al., Science **346**, 614 (2014).
7. I. Korover, N. Muangma, O. Hen et al., Phys. Rev. Lett. **113**, 022501 (2014).
8. E. Piasetzky et al., Phys. Rev. Lett. **97**, 162504 (2006).
9. A. Tang et al., Phys. Rev. Lett. **90**, 042301 (2003).
10. N. Fomin et al., Phys. Rev. Lett. **108**, 092502 (2012).
11. K. Egiyan et al. (CLAS Collaboration), Phys. Rev. Lett. **96**, 082501 (2006).
12. L.L. Frankfurt et al., Phys. Rev. C **48**, 2451 (1993).
13. L.B. Weinstein et al., Phys. Rev. Lett. **106**, 052301 (2011).
14. O. Hen, E. Piasetzky, and L.B. Weinstein, Phys. Rev. C **85**, 047301 (2012).
15. H. Gallagher, G. Garvey, and G.P. Zeller, Ann. Rev. Nuc. Part. Sci. **61**, 355 (2011).
16. B.A. Li, B.J. Cai, L.W. Chen and J. Xu, Prog. Part. Nuc. Phys. **99**, 29 (2018).
17. E. Caurier et al., Rev. Mod. Phys. **77**, 427 (2005).
18. J.J. Kelly, Adv. Nucl. Phys. **23**, 75 (1996).
19. W.H. Dickhoff and C. Barbieri, Prog. Part. Nucl. Phys. **52**, 377 (2004).
20. J. Carlson et al., Rev. Mod. Phys. **87**, 1067 (2015).
21. L.L. Frankfurt and M.I. Strikman, Phys. Rep. **76**, 215 (1981).
22. S.K. Bogner and D. Roscher, Phys. Rev. C **86**, 064304 (2012)
23. S.N. More, S.K. Bogner, and R.J. Furnstahl, Phys. Rev. C **96**, 054004 (2017)
24. B.A. Mecking et al., Nucl. Instrum. Methods A **503**, 512 (2003).
25. Online Supplementary Materials.
26. M.M. Sargsian, Phys. Rev. C **89**, 034305 (2014).

27. R.B. Wiringa, R. Schiavilla, Steven C. Pieper, and J. Carlson, Phys Rev. C **89**, 024395 (2014).

28. Jan Ryckebusch, Maarten Vanhalst, and Wim Cosyn, J. Phys. G. **42**, 055104 (2015)

29. A. Rios, A. Polls, and W.H. Dickhoff, Phys Rev C **79**, 064308 (2009).

30. M. Kortelainen and J. Suhonen, Phys. Rev. C **76**, 024315 (2007).

Author Contributions The CEBAF Large Acceptance Spectrometer was designed and constructed by the CLAS Collaboration and Jefferson Lab. Data processing and calibration, Monte Carlo simulations of the detector and, data analyses were performed by a large number of CLAS Collaboration members, who also discussed and approved the scientific results. The analysis presented here was performed by M.D. with input from O.H., E.P., and L.B.W., and reviewed by the CLAS collaboration.

The CLAS Collaboration

M. Duer,[1] O. Hen,[2*] E. Piasetzky,[1] H. Hakobyan,[3] L.B. Weinstein,[4] M. Braverman,[1] E. Cohen,[1] D. Higinbotham,[5] K.P. Adhikari,[29] S. Adhikari,[15] M.J. Amaryan,[4] J. Arrington,[6] A. Ashkenazi,[2] J. Ball,[10] I. Balossino,[20] L. Barion,[20] M. Battaglieri,[22] V. Batourine,[5, 28] A. Beck,[2] I. Bedlinskiy,[26] A.S. Biselli,[13, 8] S. Boiarinov,[5] W.J. Briscoe,[18] W.K. Brooks,[3, 5] S. Bueltmann,[4] D. Bulumulla,[4] V.D. Burkert,[5] F. Cao,[12] D.S. Carman,[5] A. Celentano,[22] G. Charles,[4] T. Chetry,[32] G. Ciullo,[20, 14] L. Clark,[40] B.A. Clary,[12] P.L. Cole,[19, 9, 5] M. Contalbrigo,[20] O. Cortes,[19] V. Crede,[16] R. Cruz-Torres,[2] A. D'Angelo,[23, 35] N. Dashyan,[43] R. De Vita,[22] E. De Sanctis,[21] M. Defurne,[10] A. Deur,[5] C. Djalali,[37] G. Dodge,[4] R. Dupre,[25] H. Egiyan,[5] A. El Alaoui,[3] L. El Fassi,[29] P. Eugenio,[16] R. Fersch,[11, 42] A. Filippi,[24] T.A. Forest,[19] G. Gavalian,[5, 30] Y. Ghandilyan,[43] S. Gilad,[2] G.P. Gilfoyle,[34] K.L. Giovanetti,[27] F.X. Girod,[5] E. Golovatch,[36] R.W. Gothe,[37] K.A. Griffoen,[42] L. Guo,[15, 5] N. Harrison,[5] M. Hattawy,[6] F. Hauenstein,[4] K. Hafidi,[6] K. Hicks,[32] M. Holtrop,[30] C.E. Hyde,[4] Y. Ilieva,[37, 18] D.G. Ireland,[40] B.S. Ishkhanov,[36] E.L. Isupov,[36] K. Joo,[12] M.L. Kabir,[29] D. Keller,[41] G. Khachatryan,[43] M. Khachatryan,[4] M. Khandaker,[31] A. Kim,[12] W. Kim,[28] A. Klein,[4] F.J. Klein,[9] I. Korover,[1] S.E. Kuhn,[4] L. Lanza,[23] G. Laskaris,[2] P. Lenisa,[20] K. Livingston,[40] I.J.D. MacGregor,[40] C. Marchand,[10] N. Markov,[12] B. McKinnon,[40] S. Mey-Tal Beck,[2] T. Mineeva,[3] M. Mirazita,[21] V. Mokeev,[5, 36] R.A. Montgomery,[40] A. Movsisyan,[20] C. Munoz Camacho,[25] B. Mustapha,[6] S. Nadeeshani,[4] P. Nadel-Turonski,[5] S. Niccolai,[25] G. Niculescu,[27] M. Osipenko,[22] A.I. Ostrovidov,[16] M. Paolone,[38] E. Pasyuk,[5] M. Patsyuk,[2] A. Papadopoulou,[2] K. Park,[5, 28] D. Payette,[4] W. Phelps,[15] O. Pogorelko,[26] J. Poudel,[4] J.W. Price,[7] S. Procureur,[10] Y. Prok,[4, 41] D. Protopopescu,[40] M. Ripani,[22] A. Rizzo,[23, 35] G. Rosner,[40] P. Rossi,[5, 21] F. Sabati´e,[10] A. Schmidt,[2] C. Salgado,[31] B.A. Schmookler,[2] R.A. Schumacher,[8] E.P. Segarra,[2] Y.G. Sharabian,[5] G.D. Smith,[39] D. Sokhn,[40] N. Sparveris,[38] S. Stepanyan,[5] S. Strauch,[37, 18] M. Taiuti,[17] J.A. Tan,[28] M. Ungaro,[5, 33] H. Voskanyan,[43] E. Voutier,[25] D.P. Watts,[39] X. Wei,[5] N. Zachariou,[39] J. Zhang,[41] X. Zheng,[6, 41] and Z.W. Zhao[4]

[1]Tel Aviv University, Tel Aviv, Israel [2]Massachusetts Institute of Technology, Cambridge, MA, 02139 [3]Universidad T´ecnica Federico Santa Mar´ia, Casilla 110-V Valpara´iso, Chile [4]Old Dominion University, Norfolk, Virginia 23529 [5]Thomas Jefferson National Accelerator Facility, Newport News, Virginia 23606 [6]Argonne National Laboratory, Argonne, Illinois 60439 [7]California State University, Dominguez Hills, Carson, CA 90747 [8]Carnegie Mellon University, Pittsburgh, Pennsylvania 15213 [9]Catholic University of America, Washington, D.C. 20064 [10]IRFU, CEA, Universit´e Paris-Saclay, F-91191 Gif-sur-Yvette, France [11]Christopher Newport University, Newport News, Virginia 23606 [12]University of Connecticut, Storrs, Connecticut 06269 [13]Fairfield University, Fairfield CT 06824 [14]Universita' di Ferrara, 44121 Ferrara, Italy [15]Florida International University, Miami, Florida 33199 [16]Florida State University, Tallahassee, Florida 32306 [17]Universita` di Genova, 16146 Genova, Italy [18]The George Washington University, Washington, DC 20052 [19]Idaho State University, Pocatello, Idaho 83209 [20]INFN, Sezione di Ferrara, 44100 Ferrara, Italy [21]INFN, Laboratori Nazionali di Frascati, 00044 Frascati, Italy [22]INFN, Sezione di Genova, 16146 Genova, Italy [23]INFN, Sezione di Roma Tor Vergata, 00133 Rome, Italy [24]INFN, Sezione di Torino, 10125 Torino, Italy [25]Institut de Physique Nucl´eaire, CNRS/IN2P3 and Universit´e Paris Sud, Orsay, France [26]Institute of Theoretical and Experimental Physics, Moscow, 117259, Russia [27]James Madison University, Harrisonburg,

Virginia 22807 [28]Kyungpook National University, Daegu 41566, Republic of Korea [29]Mississippi State University, Mississippi State, MS 39762-5167 [30]University of New Hampshire, Durham, New Hampshire 03824-3568 [31]Norfolk State University, Norfolk, Virginia 23504 [32]Ohio University, Athens, Ohio 45701 [33]Rensselaer Polytechnic Institute, Troy, New York 12180-3590 [34]University of Richmond, Richmond, Virginia 23173 [35]Universita' di Roma Tor Vergata, 00133 Rome Italy [36]Skobeltsyn Institute of Nuclear Physics, Lomonosov Moscow State University, 119234 Moscow, Russia [37]University of South Carolina, Columbia, South Carolina 29208 [38]Temple University, Philadelphia, PA 19122 [39]Edinburgh University, Edinburgh EH9 3JZ, United Kingdom [40]University of Glasgow, Glasgow G12 8QQ, United Kingdom [41]University of Virginia, Charlottesville, Virginia 22901 [42]College of William and Mary, Williamsburg, Virginia 23187-8795 [43]Yerevan Physics Institute, 375036 Yerevan, Armenia

Methods

Analysis details. The A(e,e'p) and A(e,e'n) event samples were selected by determining the common angular region for detecting both protons and neutrons, correcting for their detection efficiencies, and accounting for the different momentum resolutions. Neutron momenta were determined to an uncertainty of about 10-15% from their measured time-of-flight using the CLAS electromagnetic calorimeter. Proton momenta were determined to an uncertainty of about 1% from the curvature of their trajectories in the CLAS magnetic field. We accounted for this momentum resolution difference by: (1) selecting the desired A(e,e'p) events in high- and low-momentum kinematics, (2) "smearing" the proton momentum for each event using the measured neutron momentum resolution, and (3) using unsmeared and smeared A(e,e'p) event samples to study bin migration effects and optimize the event selection criteria. This results in a smeared event sample with as many of the 'original' A(e,e'p) events as possible (i.e. high selection efficiency), and as few other events as possible (i.e. high purity). We used the smeared proton momenta in the final selection of A(e,e'p) events for consistency with the A(e,e'n) analysis.

The final event sample contains about 85-90% of the desired sample with about 15% contamination, resulting in at most about 5% more events in our sample. This 5% cross section correction caused a less than 1% correction to ratios between different nuclei. We assigned systematic uncertainties equal to the corrections. See [25] for additional details.

Non-QE reaction mechanisms and data interpretation. As the measurement observes only the final state particles, we need to include different reaction mechanisms to infer information about the nuclear initial state. In addition to QE electron scattering from a single nucleon, the full reaction mechanism could include contributions from Meson-Exchange Currents (MEC),

Isobar Currents (exciting the struck nucleon to an excited state, IC), and elastic and inelastic nucleon rescattering (final-state interactions or FSI). In the case of high missing momentum, elastic FSI include re-scattering between the nucleons of the pair and/or with the residual system. The relative contribution of these reaction mechanisms, as compared to the QE reaction of interest, strongly depends on the reaction kinematics [2-4, 31, 34]. Minimizing non-QE reaction mechanisms also reduces their interference with the QE reaction.

The high missing momentum measurement reported here was carried out in high-Q^2, $x_B > 1$, largely anti-parallel kinematics. This kinematical region minimizes non-QE reaction mechanisms as follows [2-4, 34]: (A) MEC are suppressed by a factor of $1/Q^2$ compared to SRC and their contribution in our kinematics is small; and (B) IC are suppressed at $x_B > 1$ where, for a given Q^2, the virtual photon transfers less energy and is less able to excite the nucleon to an IC. Further, at large knockout nucleon momenta, FSI effects can be calculated using a generalized Eikonal approximation in a Glauber framework [3, 32-35]. These calculations show that, in our measurement, elastic FSI are largely suppressed for mean-field knockout. For SRC breakup, they are confined to nucleons in close proximity, and thus the majority of the cross section comes from short-range pairs [3,31].

This simple QE picture, with suppressed FSI, is strongly supported by the fact that it describes well both high-Q^2 electron scattering data and high energy proton data [8-9], which have very different reaction mechanisms. In addition, the results of the electron and proton scattering experiments give consistent SRC-pair isospin ratios [5,8,9] and center of mass momentum distributions [9,36].

Asymmetry Dependence of reaction mechanisms. As protons and neutrons propagate through asymmetric nuclei, they encounter more neutrons than protons, which could lead to different FSI effects that would not cancel in the cross-section ratios. However, at the large Q^2 of this measurement, the pp and nn scattering cross-sections are almost identical, leading to a 1% difference between proton and neutron FSI, as estimated quantitatively using a full Relativistic Multiple-Scattering Glauber Approximation (RMSGA) calculation [34].

Data interpretation using unitary transformations. From a theoretical standpoint, one can describe the scattering reaction in one of two mathematically equivalent ways: (A) using one-body operators acting on a ground state wave-function with a high momentum tail, as primarily discussed in the text, or (B) using unitary transformed many-body operators acting on a 'mean-field' ground state without a considerable high-momentum tail [23]. In the latter case the description of the ground state is simpler, but complicated many-body operators are needed to describe the electron-nucleus interaction that leads to the measured final state. While proven to be a very efficient in describing long distance / low energy properties of nuclei, it is not clear yet if this approach is a cost-effective way to describe the measured

short-distance physics in heavy nuclei. Therefore, we discuss our results predominantly in the framework of untransformed wave functions and interactions.

31. M L. L. Frankfurt, M. M. Sargsian, and M. I. Strikman Phys. Rev. C **56**, 1124 (1997).
32. C. Colle et al., Phys. Rev. C **92**, 024604 (2015).
33. D. Dutta, K. Hafidi, and M. Strikman, Prog. Part. Nucl. Phys. **69**, 1 (2013).
34. C. Colle, W. Cosyn, and J. Ryckebusch, Phys. Rev. C **93**, 034608 (2016).
35. O. Hen, *et al*., Phys. Lett. B **722**, 63 (2013).
36. R. Shneor et al., Phys. Rev. Lett **99**, 072501 (2007).